Wave climate trends and breakpoints during the Atlantic Multidecadal Oscillation (AMO) in southern Brazil

Natan Zambroni Maia[1,*], Luis Pedro Almeida[1,2], Leonardo Emmendorfer[3], João Luiz Nicolodi[1], Lauro Calliari[1]

[1] Universidade Federal do Rio Grande- Instituto de Oceanografia - Laboratório de Oceanografia Geológica - Campus Carreiros (Av. Itália - Carreiros, Rio Grande - 96201-900 - RS - Brazil)
[2] CoLAB +Atlantic - LACS Building (Estrada da Malveira da Serra, 920 - 2750-834 - Cascais Portugal)
[3] Universidade Federal do Rio Grande - Centro de Ciências Computacionais (Rodovia, RS-734, s/n - Carreiros, Rio Grande - 96203-900 - RS - Brazil)

* Corresponding author: natanzambroni@gmail.com

ABSTRACT

Understanding how wave climate variability and its trends change over time are crucial analyses required to mitigate potential wave-induced impacts and adapt coastal areas to such effects. The long-term trends and breakpoints of the wave energy flux (WEF) and its relationship with teleconnection patterns in southern Brazil were studied using ERA-5 wave reanalysis with validation using a waverider. We determined that the interannual mean WEF (WEFm) and extreme WEF (WEF98) that reaches the southern Brazil have increased over the past four decades, with a increment of 0.063 and 0.17 kW/m/year, respectively 0.63 and 0.29% per year. By the Muggeo method we determined that subperiods with increasing WEFm trends are related to the SSE and SSW quadrants and that these are also the most energetic ones and with the highest annual increment rates of WEFm and WEF98. Our results also suggest that the positive trends observed in interannual WEF values are likely related to the long term transition of cold to warm Atlantic Multidecadal Oscillation (AMO) phase in the western South Atlantic Ocean. From a coastal risk perspective, it is important to understand the relationship between climatic indices and the wave climate to support long-term coastal management policies.

Descriptors: Wave hindcast, ERA-5 reanalysis data, Western South Atlantic Ocean, Wave energy flux, Climate indices.

INTRODUCTION

Climate changes, including modifications in wind patterns, will lead to changes in the wave climate that could affect coastal erosion and flooding processes (Mentaschi et al. 2017; Garner et al. 2017; Rasmussen et al. 2018; Vousdoukas et al. 2018; Oliveira et al. 2019a). Understanding how wave characteristics (e.g., the wave height, period, direction and energy) change over time

and their long-term trends is crucially required to mitigate potential hazards and allow low-lying coastal areas to adapt to such threats. Therefore, the evaluation of trends in future wave climates is fundamental for the development of efficient policies within the framework of climate change adaptation and mitigation measures (De Leo et al. 2021). Previous studies in the Atlantic Ocean have shown a consensus that the northern part of the North Atlantic Ocean has presented a trend of increasing storminess and mean significant wave height (Kushnir et al. 1997; Wang and Swail 2000; Swail et al. 2000; Wang et al. 2003; Dodet et al. 2010; Mentaschi et al. 2017). Further north, in the Arctic Ocean, Waseda et al. (2018) also found a

trend of increasing wave heights over the past four decades. Recent studies based on global climate change projections indicate that in the mid-latitude oceans, the wave height and period will increase and the mean wave direction will shift from 5–15° to the north due to changing patterns of storm wind speeds (Hemer et al. 2006; Mori et al. 2010; Semedo et al. 2011; Morim et al. 2019).

Wave measurements in the South Atlantic Ocean are very scarce and, in most cases, consist of occasional short-term observations. For this reason, most previous studies that have investigated trends in the wave climate in the South Atlantic were performed based on hindcast or forecast datasets. According to Reguero et al. (2013) and Oliveira et al. (2019a), increasing trends in significant wave heights were identified in the western South Atlantic over the past 60 and 32 years, respectively. By investigating wave energy flux (WEF) projections using global-scale modeling, the study performed by Mentaschi et al. (2017) found that by the end of this century, there will be a significant increase (up to 30%) in the 100-year return level of the WEF in the majority of coastal areas in the southern temperate zone, including the Southwest Atlantic Ocean. Using in-situ buoy data and model data Pegorelli et al. (2018) identified that the Atlantic coast of Brazil has a moderate wave power, once during all the months of the year, the WEF was consistently estimated within the 10 to 30 kW/m range, with the majors WEF values under influence of the passage of cold front systems, with strong winds from the SSW (Rodrigues et al., 2004; Dominguez, 2006).

According to Silva et al. 2020, wave direction oscillations coexist with long-term variations in interhemispheric surface temperature anomalies, which indicates the influence of temperature-driven atmospheric teleconnections on wave generation cycles. For instance, Reguero et al. (2019) found inter-regional correlation of 0.54 between sea surface temperature (SST) variations in North and tropical Atlantic and WEF variations in extratropical South Atlantic. The global climate has preferred patterns of variability, called climate modes. Climate modes, such as the Southern Annular Mode (SAM), El Niño–Southern Oscillation (ENSO) and the Atlantic Multidecadal Oscillation (AMO), are widely considered to be associated with typical natural climate variability at interannual to multidecadal scales, which is mainly reflected in variations in the patterns and distributions of the sea level pressure (SLP), wind and SST (Thompson and Wallace 1998; Kerr 2000; Trenberth et al. 2002; Hurrell et al. 2003; Hemer et al. 2010; Silva et al. 2020). The wave climate variability in different parts of the globe is modulated by one or a combination of several climate modes; thus, reliable projections of wave characteristics require an in-depth understanding of the relationships between climate modes and the wave climate.

Described by Kerr (2000), the AMO is seen as an indicator of global overturning circulation changes (Biastoch et al. 2015), particularly those related to thermohaline circulation variations. The AMO has been identified as a coherent mode of natural variability occurring in the Atlantic Ocean based upon the average anomalies of SST in the North Atlantic basin, typically over 0-70N and is dominated by multidecadal variations with lest than 0.4 °C of magnitude range alternating between warm (positive) and cold (negative) phases with a periodicity of approximately 70 years and and 0.4 °C of anomaly to global SST (Wang et al. 2009; Frajka-Williams et al. 2017; Kayano et al. 2019; Trenberth & Shea 2006; Trenberth et al. 2021). Warm AMO phases occurred during 1870–1900 and 1925–1963, and cold phases occurred during 1900–1925 and 1963–1995. Since 1995, the AMO has been positive in a new warm phase (Ortega et al. 2013; Alexander et al. 2014).

The imprints of the AMO on the SST and SLP fields, although centered in the North Atlantic, extend well beyond this area and have pronounced influences on weather and climates throughout the world. The AMO largely affects global climate change (Yang et al. 2020), and different effects observed across the globe, such as temperature and pressure variations in the South Atlantic and Pacific, which is a zonally elongated band in the Southern Ocean and in the tropical Pacific, as well as warming in the north and southwest Pacific (Lyu and Yu 2017; Odériz et al. 2020), could be pacemakers of the global air temperature (Kravtsov and Spannagle, 2008). As one of the most important

climate modes, the AMO has been widely linked to prominent regional climate anomalies that can have tremendous worldwide socioeconomic consequences, as in the Asian, Indian and South American monsoons (Zhang and Delworth, 2005; Chiessi et al. 2009), summer drought pattern in China (Qian et al. 2014), Siberian rainfall (Sun et al. 2015), low-frequency El Niño–Southern Oscillation modulations (Timmermann et al. 2007), and changes in rainfall and temperatures over the United States, Australia, Europe and northeast Brazil (Knight et al. 2006; O'Reilly et al. 2017), in addition to modulating Atlantic hurricane and tropical cyclone activity (Goldenberg et al., 2001; McCabe et al., 2004; Wang et al. 2008), wave power in the Southern Ocean (Reguero et al. 2019) and affecting the abundance of fish populations in the Mediterranean and North Atlantic (Alheit et al. 2014).

By concentrating the analyses on the Atlantic, we observe that the AMO effects are felt throughout the ocean, imparting dipole behavior, wherein the warm AMO phase features anomalously warm the North Atlantic and anomalously cool the South Atlantic and Southern Oceans, with strong meridional gradients in the 40°-70°S band, while the cold AMO phase shows an almost reversed-sign SST anomaly pattern (Timmermann et al. 2007; Wang et al. 2008; Latif 2013; Lyu and Yu 2017; Kayano et al. 2019; Reguero et al. 2019). This behavior supports the hypothesis that the driving mechanism of the AMO involves fluctuations of the Atlantic meridional overturning circulation (AMOC) (Delworth and Mann, 2000; Knight et al., 2005; Dijkstra et al., 2006). As the AMOC is enhanced, warming and cooling occur in the North and South Atlantic, respectively, and the opposite is observed with a reduction in the AMOC. According to Crowley and Kim (1993), decadal to multidecadal changes in the thermohaline circulation should primarily affect temperatures in the Atlantic and Southern Ocean, with a clear signature in the SST field in the Weddell Sea and Drake Passage, in addition to changes that are almost out-of-phase between the Northern and Southern Hemispheres.

In the South Atlantic Ocean, previous studies based on wave and SST reanalysis data (Ortega et al. 2013; Alexander et al. 2014; Biastoch et al.

2015; Kayano et al. 2019) have revealed strong relationships between changes in ocean–atmosphere interactions and the AMO index. Studies developed by Biastoch et al. 2015 in the Southeast Atlantic determined that Agulhas leakage and the AMO are correlated and covary on multidecadal timescales. Kayano et al. (2019) demonstrated that in general, the SST anomaly patterns feature nearly zonal structures along the southern midlatitudes, with strong meridional gradients in the South Atlantic. According to these authors, AMO-related large-scale SST anomaly patterns play an important role in cyclone trajectories and the Lorenz energy cycle; thus, low-level cyclones in the South Atlantic are clearly modulated by the AMO, becoming even more energetic in the warm AMO phase than in the cold AMO phase.

Therefore, it is possible to infer that SST meridional gradients alter the longwave baroclinicity, which in turn takes part in the energy cycle in the South Atlantic. During the negative and positive AMO phases, heat flows in ocean–atmosphere interactions induce changes in available potential and kinetic energies, low-level extratropical cyclones, wind patterns and, consequently, the wave climate in the western South Atlantic (Escobar et al. 2004; Ortega et al. 2013; Kayano et al. 2019).

Although general linear trends are known, little is known about the temporal variability in the WEF and its relationship with the AMO in the Southwest Atlantic. As previously demonstrated, the wave climate in this region is under the strong influence of teleconnection patterns. Therefore, WEF trend analyses associated with climate indices, not only linear analyses but also analyses considering breakpoints, provide relevant to contributions to the understanding of WEF behavior in the Southwest Atlantic Ocean, including possible oscillatory behavior. Based on the aforementioned theoretical background, the present study aims to investigate the long-term trends and breakpoints of the WEF in the western South Atlantic using 41 years (from 1979 to 2019) of reanalysis data (ERA-5). The work was divided into two sections: 1) validation of the ERA-5 dataset, wherein wave parameters from ERA-5 reanalysis were compared with those of waverider observations, and 2) historical WEF analysis considering trends and

breakpoints, with an investigation of the relationship between WEF temporal variability and the AMO index. To the best of our knowledge, the Southwest Atlantic WEF variability and its relationship with the AMO documented herein have not been described previously.

METHODS

Study area

The present study focuses on the wave climate in the southwestern Atlantic Ocean, specifically on the extreme southern coast of Brazil (Rio Grande do Sul). Southern Brazil is under the influence of two main systems: the South Atlantic Semifixed Tropical Anticyclone (ATAS) and the Migratory Polar Anticyclone (APM). The swell generally comes from the S/SW (longer waves) and wind-sea varies from NE (shorter waves) under the influence of extratropical cyclones ATAS and from S/SE to S/SW in the presence of extratropical cyclones (Pereira et al. 2017). The seasonaly alternation between these two systems favors the predominance of winds from the northeast (NE) during September through March (ATAS) and the southwest (SW) during April through August (APM) (Godolphin 1976). In addition, it is important to note that the region between the Antarctic Peninsula and southern Brazil has the highest rate of cyclone formation in the Southern Hemisphere (Hoskins and Hodges 2005; Pezzi et al. 2016).

According to the global dynamic classification of coasts proposed by Davies (1964) and King (1972), the Rio Grande do Sul coast is characterized as exhibiting "east coast swell" (Calliari and Klein 1993). Long-period waves with high sediment transport capacity, which are usually formed in the subpolar stormy belt and over the Drake Passage, occur predominantly from the southeast (SE) and less frequently from the south (S) due to the more frequent and strong cyclones in the former direction (Tomazelli and Villwock 1992; Gonzales et al. 2016). Sea waves, which are generated by local winds, come mainly from the east (E) and northeast (NE) and are related to the prevailing winds in the region. Storm waves have a lower frequency of occurrence and are formed by strong winds from southern quadrants during extreme

meteo-oceanographic events (Motta 1969; Maia et al. 2016).

On the Rio Grande do Sul coast, waves exhibit a directional bimodality distribution (Pereira et al. 2017).. According to Pianca et al. (2010), during the summer, the predominant wave directions are from the NE (28.4%) and S (26.7%), with NE waves presenting heights between 1 and 2 m, with periods between 6 and 8 s, and S waves presenting heights between 1 and 3 m, with periods from 8 to 12 s. In autumn and winter, the dominant wave direction is from the S (36.7%), with heights between 2 and 3 m and periods between 10 and 12 s. In the spring, NE waves are dominant, with heights between 1 and 3 m and periods from 6 to 8 s, although an important contribution from S waves with heights between 1 and 3 m and periods from 8 to 10 s still occurs.

ERA-5 wave data

Wave data were obtained from the ERA-5 reanalysis dataset (Hersbach et al. 2020; Copernicus Climate Change Service (C3S) 2017) covering 41 years (from 1979 to 2019) and we used a 3-h temporal resolution to calculate annual averages for an Eulerian analysis from a single point located at the coordinates 32°30'S/50°W at a 1000 m depth (deep waters) (Figure 1).

The ERA-5 reanalysis is a global atmospheric, wave and ice data assimilation system that provides free products ranging from 1979 to the present in a near real-time scheme and is maintained by the European Centre for Medium-Range Weather Forecasts – ECMWF. ERA-5 wave data are generated by the WAM, which is a 3rd-generation model that integrates the basic transport equation describing the evolution of a two-dimensional ocean wave spectrum without additional unplanned assumptions regarding the spectral shape. The WAM uses altimeter wave height and advanced SAR observations as the source in the model assimilation and ETOPO2 as a bathymetry database from the National Geophysical Data Center (NGDC/NOAA).

There are three explicit source functions that describe the wind input, nonlinear transfer and whitecapping dissipation. There is an additional bottom dissipation source function, and refraction
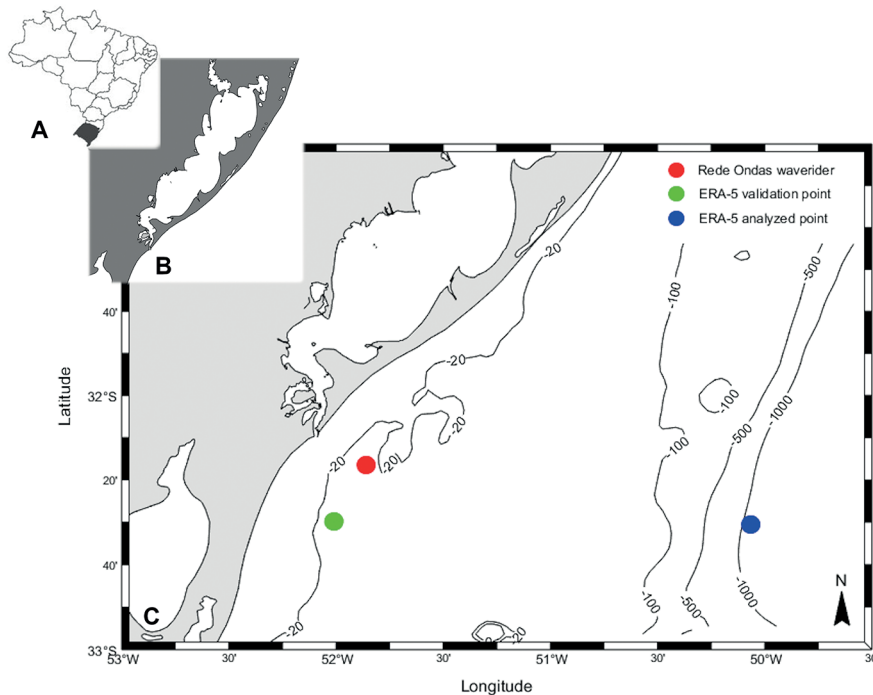
Figure 1. Locations of the Rede Ondas waverider, ERA-5 validation point and ERA-5 analyzed point.

terms are included in the finite-depth version of the model, so it takes in account for basic shallow water physics, namely the maximum wave energy and the frequency down shifting are controlled by the water depth. The model runs on a spherical latitude-longitude grid and can be used in any ocean region. The WAM predicts directional spectra along with wave properties such as the significant wave height, mean wave direction and frequency, swell wave height and mean direction, and wind stress fields corrected by including the wave-induced stress and the drag coefficient at each grid point at chosen output times (The Wamdi Group 1988; Dee et al. 2011). The slow attenuation of long-period swells and the impact of shallow water on the wind input are introduced with the overall return of the level of dissipation due to white capping. Taking into account that the model uses data assimilation in intermediate waters, its products consider the wave transformations induced by the variation of depth and interaction with the bottom. However, it is worth mentioning that due to the 0.5° grid resolution of the model, bathymetric variations smaller than this scale may not be well represented and cause uncertainties in some

results, such as the wave direction. A detailed description of ERA-5 may be found in Hersbach et al. (2020). ERA-ECMWF reanalysis data have been extensively used in other studies to provide relevant results (Hoskins and Hodges 2005; Harley et al. 2010; Semedo et al. 2011; Vousdoukas et al. 2018; Waseda et al. 2018; Wan et al. 2018).

COMPARISON BETWEEN ERA-5 AND IN SITU OBSERVATIONS FROM A WAVERIDER

To validate the ERA-5 data base for our region of interest, wave observations from a local waverider (model Mark III -Datawell) from the Rede Ondas Project (www.redeondas.furg.br), which is part of the Global Ocean Observation Program (GOOS-UNESCO), were used. The waverider is located at coordinates 32°20'23''S/51°53'53''W and we compared it with another ERA-5 point at coordinates 32°30'S/52°W. These points are 20 km apart and are 25 m of deep (Figure 1). Both ERA-5 and waverider data comprise measurements of significant wave height (Hs), mean period (T), and mean wave direction (θ). After validation of the ERA-5 the WEF was computed for our point of interest at 1000m depth following Equation 1:

$$\text{WEF} = \frac{\rho g^2 Hs^2 T}{64\pi}$$

Equation 1

where ρ is the water density (kg/m^3), g is the gravitational acceleration (m/s^2), Hs is the significant wave height (m), and Te is the energy period (s). The energy period (Te or T-10) can be estimated from the spectral shape and other parameters. The mean period (T or T01) and the energy period can be related through the Equation 2:

$$\text{T}e = \frac{m_{-1}}{m_o} = \alpha T$$

Equation 2

where α depends on the spectral shape. Here, α is assumed to be 0.538 (Reguero et al. 2015; Antolínez et al. 2016; Reguero et al. 2019). The WEF provides an indication of the potential wave energy (combining both the wave period and height) that can reach the coast and has been widely used in wave climate studies (Antolínez et al. 2016, Mentaschi et al. 2017, Marshall et al. 2018, Reguero et al. 2019, Odériz et al. 2020). To compare both datasets, continuous hourly records covering nine months of 2016 (excluding March, November and December) were used. To evaluate the quality of the comparisons, three statistical parameters were calculated: Pearson's correlation coefficient (R; at a 95% confidence interval), the root mean square error (RMSE) and the bias of the fit. The "R" parameter measures the possible degree of relation between two variables, the RMSE determines the average magnitude of the difference between an estimated and true value, and bias evaluates the differences between measured and simulated data (zero bias means that the predictor parameter is unbiased).

WAVE CLIMATE TRENDS

For the analysis of 41 years of ERA-5 wave climate data (from 1979 to 2019), the data were separated into four directional sectors containing only the waves that affect the coastal zone, considering the distinct wave climate forcing sources that affect this region and the coastline orientation (NE-SW) (Tomazelli and Villwock 1992; Gonzales et al. 2016; Motta 1969; Maia et al. 2016; Pianca et al., 2010). The annual mean and 98th percentile of the WEF were computed for the 41-year

ERA-5 data, and long-term linear trends were calculated using a linear regression model at a 95% confidence level. The statistical significance of long-term trends was verified through an analysis of variance (ANOVA) at a 95% confidence level. ANOVA is a statistical tool that defines whether the mean values of any variable are significantly different from each other (critical F < F; P < 0.05).

SEGMENTED LINEAR REGRESSION AND BREAKPOINT DETECTION

In this paper, to identify changing trends in WEF time series, we used a method proposed by Muggeo (2003) to fit segmented relationships in regression models. Thus, it was possible to identify breakpoints indicating that there were statistically significant changes in the behavioral trends of the WEF time series analyzed. Segmented linear regression represents a dependent variable Y as a piecewise linear function of an independent variable X. The values of X that determine changes in the linear models are called breakpoints, which can be determined by the iterative Muggeo method. For each breakpoint BPk detected, two linear models consistent with the input data are inferred (Eq. 3 and Eq. 4):

$$\mathbf{Yr} = \mathbf{\beta 1.X + c1} \text{ for } X < \text{BPk}$$

Equation 3

$$\mathbf{Yr} = \mathbf{\beta 2.X + C2} \text{ for } X > \text{BPk}$$

Equation 4

where Yr is the piecewise linear estimation of variable Y, $\beta 1$ and $\beta 2$ are the slopes of the linear models, and c1 and c2 are the constant coefficients of the linear models.

The detection of breakpoints occurs as follows. For a single variable, the residuals resulting from the linear model are normalized by dividing them by their corresponding standard deviation. The normalized residuals are represented by a segmented linear model, giving rise to subperiods, wherein breakpoints are detected using the Muggeo (2003) method. Each segmented linear model is submitted to a F-Test to compare variances, and its p-value at a 95% confidence level indicates whether there is any significant trend in each analyzed

subperiod. The number of breakpoints is increased iteratively while the method converges, and the final number of breakpoints is reported as the result. For a pair of variables or even a larger group, the procedure is the same, except that the normalized residuals from all variables considered are aggregated under the same series.

AMO INDEX

Based on its influence across the Atlantic Ocean, the AMO index was used to represent large-scale processes that may influence climatic conditions in the South Atlantic and was obtained from the National Oceanic and Atmospheric Administration (NOAA). The AMO dataset consists of gridded average anomalies of the Kaplan SST in the North Atlantic basin over 0–70N from 1856 to the present derived from UK Met Office SST data subjected to sophisticated statistical techniques to fill gaps (NOAA; Enfield et al. 2001). To investigate the relationship between the WEF temporal variability and the AMO, a time-window filter of 10 years (Enfield et al. 2001; Lyu and Yu 2017) was applied to both the WEF and AMO datasets. Following this filter, the linear correlation between the WEF annual mean (WEFm), 98th percentile (WEF98) and the AMO index were calculated according to Oderiz et al. (2020), where the range of values for the correlation coefficient was denoted as follows: 0 indicates no relationship between the variables; values between 0 and 0.25 (– 0.25 and 0) indicate a weak positive (negative) correlation; values between 0.25 and 0.5 (– 0.5 and – 0.25) have a moderate positive (negative) correlation; values between 0.5 and 0.75 (– 0.75 and – 0.5) show a strong positive (negative) correlation; and values be- tween 0.75 and 1.0 (– 1.0 and – 0.75) indicate a very strong positive (negative) correlation.

RESULTS

ERA-5 WAVE DATA VALIDATION

The correlation between ERA-5 wave data and waverider measurements indicates good agreement between the majority of compared data (Table 1). Of all compared wave parameters, Hs showed the highest correlation (R = 0.82) and lower RMSE value (0.41), with ERA-5 showing a great ability to capture extreme events (as observed in October 2016) and mean wave heights with similar quality (Table 1 and Figure 2). The bias value indicated that ERA-5 tends to overestimate Hs values by 0.22 m.

The T results showed a value of RMSE=2.79 and a correlation value of R = 0.55, which was considered statistically moderate. The T bias value showed that, on average, ERA-5 underestimated the waverider observations by 0.71 s. The θ showed a slightly higher R value of 0.6, also indicating a moderate agreement between both datasets (Table 1) and the highest value of RMSE, 39.49.

A statistical comparison between the mean and standard deviation (stdv) values computed for the entire validation dataset showed that ERA-5 presented an average Hs value of 1.44 m (stdv=0.54) and T of 8.79 s (stdv=2.34), which were close to the mean values computed based on waverider observations, at 1.22 m (stdv=0.57) and 9.5 s (stdv=3.16), respectively. For the wave direction, the mean values were similar under the predominant wave direction as the SE quadrant (147.2° for the waverider (stdv=23.49) and 137.6° for ERA-5 (stdv=47.44)), which was an expected result, considering that the time series used for this comparison does not include summer months (March, November and December), when

Table 1. Statistical results of the comparison between ERA-5 reanalysis data and Rede Ondas waverider data using nine months of records from 2016 (n=5575 for each parameter). Hs= significant wave height; Tp= peak period; θ= mean wave direction; R= Pearson's correlation coefficient; RMSE= root mean square error.

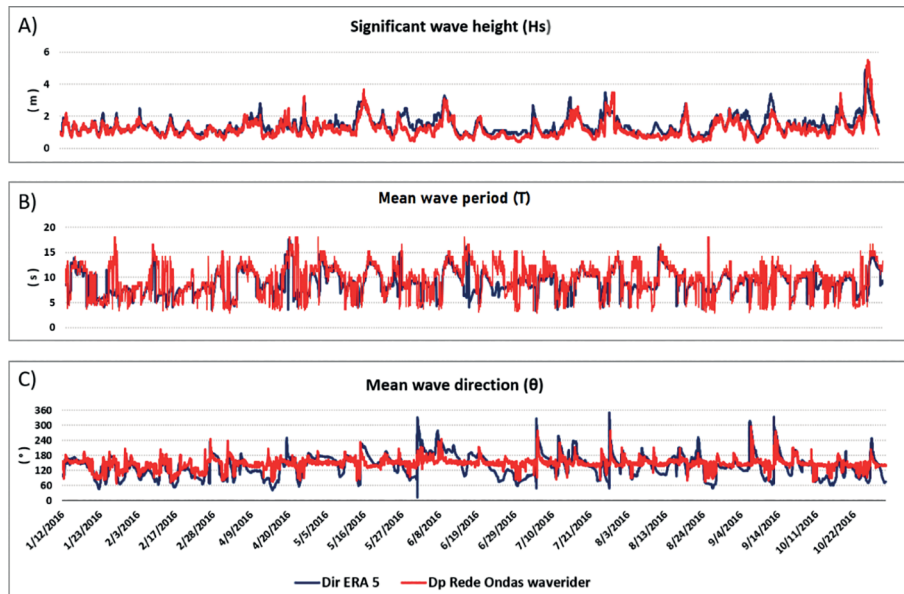| Parameter	R	RMSE	BIAS
Hs (m)	0.82	0.41	+0.22
Tp (s)	0.55	2.79	-0.71
θ (°)	0.6	39.49	-

Figure 2. Time series of overlapping Hs (A), T (B) and θ (C) from ERA-5 and Rede Ondas waverider data during 2016.

waves from northern directions are more frequent (Pianca et al. 2010). In addition to this fact and as already pointed out, it is important to consider that some bathymetric features and consequently the refraction processes may not be well represented by the model and thus, the validation process between waverider and ERA-5 may contain inaccuracies. Since refraction reduces the variability of direction towards the coast and tends to keep them in an alignment perpendicular to it, waves registered by waverider seems to be more affected by refraction than waves in the ERA-5 node. This fact can be observed in the higher values of stdv associated with the model data than those associated with that observed by the buoy (47.44 x 23.49) and may also explain the lower correlation value associated with the two databases (R=0.6) as well as its highest RMSE value (39.49).

Despite these potential inaccuracies, in general, the ERA-5 data well represented the values of Hs, T and θ recorded by the Rede Ondas waverider. The high resolution of the hindcast, as well as its validation against in-situ measurements, brings confidence to the data base, particularly for its use in long term and average conditions analysis, as is the case here.

ERA 5 COMPARISONS FOR SOUTHERN BRAZIL

The ERA-5 wave data effectively represented the Hs, T and θ values recorded by the Rede Ondas waverider. The comparison with other studies that performed validation tests between reanalysis data and in situ measurements is shown in Table 2. As already pointed out by Almeida et al. (2011), these results sometimes differ from other previous studies, probably due to factors such as the different modeling strategies used (e.g., the resolutions of wind fields and model grids) and varying dataset lengths, areas and time periods but, in general, they present similarities between the correlation values of the analyzed variables. The results presented herein, as quantified by the different statistical analyses performed, are similar to comparisons performed in previous studies in different oceans around the globe (Table 2). The statistical evaluation of ERA-5 wave reanalysis performed in the present work provides a high level of confidence that this dataset can be used in this region of the South Atlantic to analyze wave climate variability and trends.

According to Waseda et al. 2018 and Oliveira et al. 2019a, the validation analysis showed that the model skill in hindcasting Hs is higher

Table 2. Statistical validation parameters found in the current work and by other authors, including the database and locations of each study. Hs= significant wave height; T= mean period; θ= mean wave direction; R= Pearson's correlation coefficient; RMSE= root mean square error.

	Present work, ERA-5, Southern Brazilian coast		Almeida et al. (2011) Wave Watch III, Portuguese coast		Wan et al. (2018) ERA-Interim, China sea		Waseda et al. (2018) ERA-Interim, Artic sea		Oliveira et al. (2019a) Wave Watch III, Southern Brazilian coast		Odériz et al. (2020) ERA-5, Pacific Ocean	
Parameter	**R**	**RMSE**	**R**	**RMSE**	**R**	**RMSE**	**R**	**RMSE**	**R**	**RMSE**	**R**	**RMSE**
Hs (m)	0.82	0.41	0.86	0.36	0.95	0.36	0.91	0.78	0.86	0.34	0.8	0.5
T (s)	0.55	2.79	-	-	0.78	0.76	-	-	0.69	1.4	-	-
θ (°)	0.6	39.49	-	-	-	-	-	-	0.69	38	-	-

than its ability to reproduce T and θ, as noted in the "R values" in Table 2. According to these authors, this result may be related to the fact that the wind resolution used to force the model might not have accurately represented the bimodal condition of the sea in the region since it is influenced by local winds.

In this validation process, it is worth mentioning that in both the ERA-5 and Rede Ondas waverider data recorded on October 28 and 29, 2016, the Hs was larger than 5 m, which was the result of the strongest coastal storm in the last 40 years in the region, and the waves were responsible for a large amount of beach erosion (Oliveira et al. 2019b).

WAVE CLIMATE TRENDS

To analyze the WEF behavior between 1979 and 2019, we calculated the long-term linear trends using linear regression models. In an analysis considering all incident wave directions (ENE-SSW), the results from the regression analysis using 41 years of wave data indicated that the linear trends observed in WEFm and WEF98 records were statistically significant (p-value < 0.05) (Table 3). Over the analyzed periods, the general WEFm and WEF98 presented an ascending trends (Figure 3), with an increment rate of 0.063 and 0.17 kW/m/year respectively.

Table 3. P-values from regression analyses of WEFm and WEF98 from the ERA-5 database tendency analysis. WEFm=mean wave energy flux; WEF98= extreme wave energy flux (98th percentile).

Parameter	p-value	Linear Trend
WEFm	1.2×10^{-7}	+0.063 kW/m/year (0.63% /year)
WEF98	1.24×10^{-2}	+0.17 kW/m/year (0.29% /year)

In addition to the analysis covering all quadrants in the same series, the WEFm and WEF98 were calculated separately for each quadrant. As shown in Table 4, the SSW quadrant presented the most energetic waves under both mean and extreme conditions (17.21 and 83.53 kW/m, respectively), in contrast to ENE waves, which were less energetic (7.37 and 40.33 kW/m, respectively). As waves begin to come more from the south, the WEFm and WEF98 associated with the waves become greater.

We also performed an ANOVA for WEFm and WEF98, referring to all directional occurrences of incident waves: the ENE, ESE, SSE and SSW quadrants. According to Table 5, we observed that there were relevant variations in the WEFm associated with waves coming all quadrants (F>critical F and p-value <0.05) and that they presented increase rates close to those of the general WEFm, at 0.054, 0.059, 0.073 and 0,094 kW/m/year, respectively. As the waves come more from the south, the greater is the annual WEFm increment associated with them. When isolated, all quadrants under extreme conditions (WEF98) showed no significant linear trend (F<critical F and p-value> 0.05).

LINEAR TRENDS AND BREAKPOINTS

Based on variations over the 41 analyzed years, we applied the Muggeo (2003) method for the normalized residual from the linear WEFm and WEF98 models. The breakpoints indicated that the surrounding subperiods presented different trends. Subperiods with continuous lines showed significant variations within the subperiod itself (with trend; p-value<0.05), and subperiods
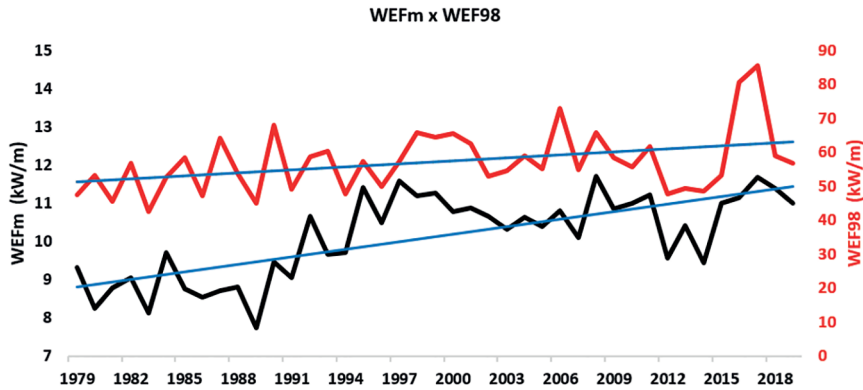
Figure 3. WEF variation between 1979–2019. The black and red lines indicate WEFm and WEF98 variations during all analyzed periods, respectively. The blue continuous lines indicates the significant growth trend of the WEFm and WEF98. WEFm=mean wave energy flux; WEF98= extreme wave energy flux (98th percentile).

Table 4. WEFm and WEF98 associated with each quadrant. WEFm=mean wave energy flux; WEF98= extreme wave energy flux (98th percentile).

	ENE (45–90°)	ESE (90–135°)	SSE (135–180°)	SSW (180–225°)
WEFm (kW/m)	7.37	8.51	10.6	17.21
WEF98 (kW/m)	40.33	44.15	47.31	83.53

Table 5. ANOVA for the WEFm and WEF98 of all wave incidence quadrants. WEFm=mean wave energy flux; WEF98= extreme wave energy flux (98th percentile); F= F-statistics.

Parameter	F	critical F	p-value	Linear Trend
WEFmENE	13.07	2.84	4.3×10^{-6}	+0.054 kW/m/year
WEFmESE	9.42	2.83	7.76×10^{-5}	+0.059 kW/m/year
WEFmSSE	18.44	3.23	2.11×10^{-6}	+0.073 kW/m/year
WEFmSSW	11.33	2.84	$1,63 \times 10^{-5}$	+0.094 kW/m/year
WEF98ENE	2.63	4.08	1.1×10^{-1}	-
WEF98ESE	2.34	4.08	1.34×10^{-1}	-
WEF98SSE	0.38	4.08	5.44×10^{-1}	-
WEF98SSW	7.89×10^{-3}	2.84	9.99×10^{-1}	-

with segmented lines did not present significant variations within the subperiod (without trend; p-value>0.05) (Figures 4 and 5). We identified three and two breakpoints for the WEFm and WEF98, respectively, which indicated that there were significant changes in the behavioral trends of both parameters. Figure 4 indicates the WEFm breakpoints in 1989, 1997 and 2014 which are the boundaries of the 1979–1989 (I), 1989–1997 (II), 1997–2014 (III) and 2014-2019 (IV) subperiods that presented alternating behaviors regarding the decreasing and increasing trends of the WEFm. Subperiod (I) was characterized by a decreasing

trend, followed by subperiod (II) with an increasing trend lasting 10 years. The following subperiod (III) of 18 years showed a downward trend between 1997 and 2014 and the last subperiod (IV) showed upward trend for the last 5 years of the time serie. The first three subperiods showed statistically significant variations in their trends with (continuous line), with p-values=0.04, 0.01 and 0.0001 while the last subperiod didn't show statistically significant trend (segmented line; p-value=0.26) Regarding the WEF98 trends, we identified two inflection points, 2008 and 2012, which delimit the following subperiods: 1979–2008 (I), 2008–2012
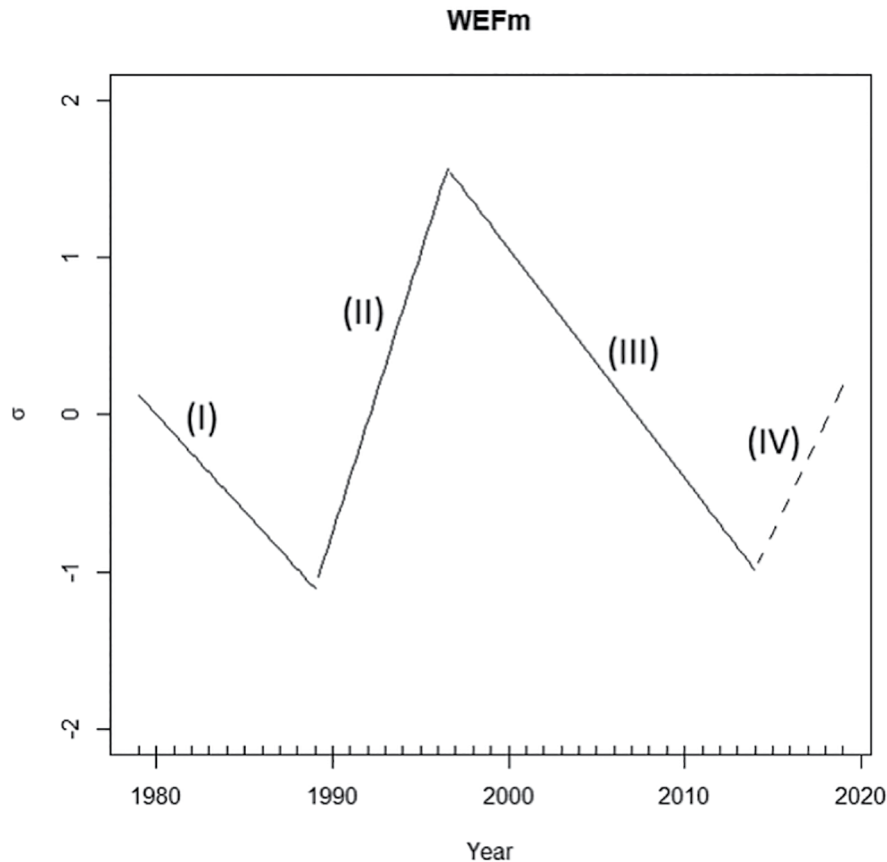
WEFm

Figure 4. Segmented linear model of the normalized residuals from WEFm linear models. Continuous lines indicate subperiods with significant variations and segmented lines indicate subperiod without significant variations. WEFm=mean wave energy flux.

(II), and 2012–2019 (III) (Figure 5). Similar to the WEFm, the WEF98 presented alternating oscillations between positive and negative trends,but all subperiods, (I), (II) and (III), did not present statistically significant trends (segmented line; p-values=0.32, 0.11 and 0.26, respectively).

Although the WEFm presents oscillatory behavior (Figure 4), there was a statistically significant and generally positive trend between 1979 and 2019 (Table 3, Figure 3), and Table 6 indicates that the mean WEFm in each subperiod identified by the Muggeo method increased over the 41 years. Subperiod (I) presented 8.71 kW/m as the mean WEFm, subperiod (II) presented a value of 9.98 kW/m, while subperiod (III) presented a higher value at 10.71 kW/m and subperiod (IV) had the largest WEFm overall, at 10.95 kW/m. Thus, by presenting the 4 subperiods with mean values of WEFm in a gradually

increasing way, Muggeo analysis reinforces the result found of the increasing tendency of general WEFm indicated in Figure 3. The mean values of each WEF98 subperiod identified by the Muggeo method (Figure 5) are adjusted in Table 7 and also present average values in an increasing manner for each sub-period, then 56.3 (I), 57. 86 (II) and 60.1 (III), reinforcing the positive trend found in the general behavior of WEF98 over the 41 analyzed years (Figure 3). We decomposed WEFm and WEF98 into four different quadrants, and through Figs. 6 and 7, it is possible to observe that all quadrants presented breakpoints throughout their time evolution, indicating that there were subperiods with different behavioral tendencies regarding variations in wave energy. For the WEFm (Figure 6), only the ENE quadrant didn't show at least one subperiod with a significant negative or
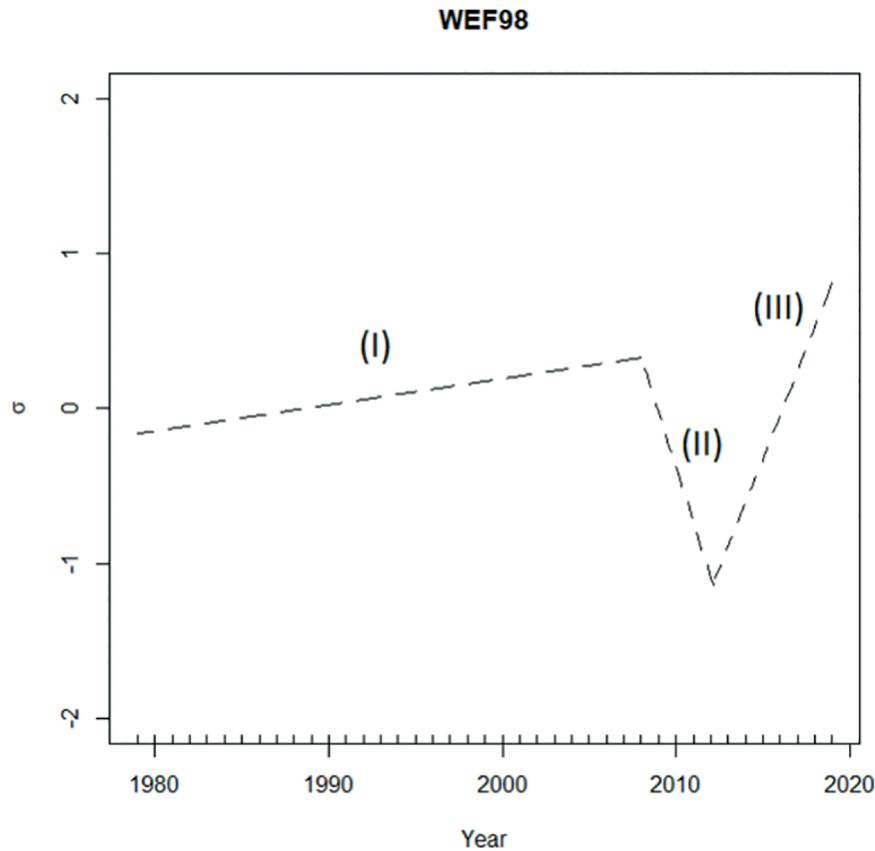
WEF98

Table 6. WEFm values for the subperiods defined by the breakpoints identified using the Muggeo method. WEFm=mean wave energy flux.

Period	1979–1989 (I)	1989–1997 (II)	1997–2014 (III)	2014-2019 (IV)
WEFm (kW/m)	8.71	9.98	10.71	10.95

Table 7. WEF98 means for the subperiods defined by the breakpoints identified using the Muggeo method. WEF98= extreme wave energy flux (98th percentile).

Period	1979–2008 (I)	2008-2012 (II)	2012–2019 (III)
WEF98 (kW/m)	56.3	57.86	60.1

positive trend (continuous line). Negative subperiods were associated with the ESE quadrant between 1997–2013,SSE quadrant between 1999–2019 and SSW quadrant between 1992-2013 Positive trends were associated with the ESE quadrant between 2013–2019, SSE quadrant between 1989-1999 and the SSW quadrant between 1986–1992.

Regarding WEF98 (Figure 7), all subperiods of all quadrants showed growth and decreasing trends without statistical significance (segmented line).

WEF VARIABILITY AND THE AMO INDEX

In Figure 8, it is possible to observe that since the 1970s, the AMO index has been increasing,
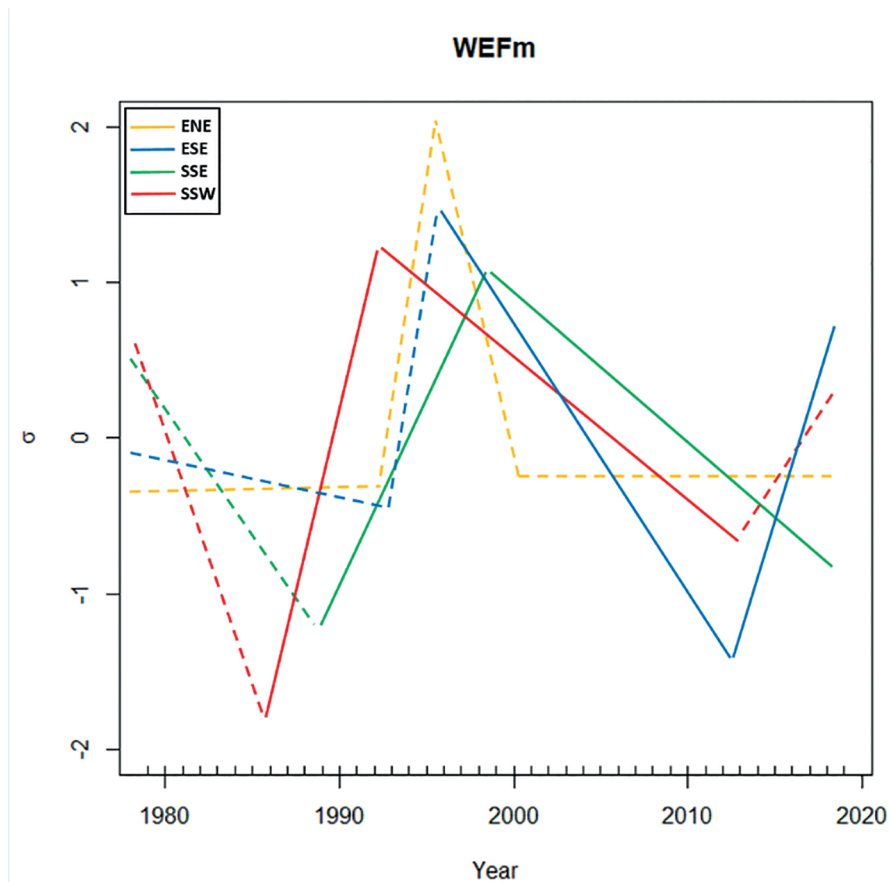
Figure 6. WEFm variation per quadrant. Continuous lines indicate subperiods with significant variations, and segmented lines indicate subperiods without significant variations. WEFm=mean wave energy flux.

shifting to a warm phase in the late 1990s. For the WEFm (Figure 8A), the results show that the 10-year running mean was very well synchronized with this AMO transition, as expressed by the very strong correlation coefficient obtained between the variables (R = 0.92, 95% significance level). For extreme energy conditions, the correlation between the 10-year running mean WEF98 and AMO was also very strong, at R= 0.89. As demonstrated by Odériz et al. (2020), R values between 0.75 and 1 indicate a very strong positive correlation between the WEF and AMO. Both curves have good synchrony with the AMO curve, showing similar behavioral trends, but in 2002, while the AMO stabilized with a small increasing trend, the WEF98 showed a decreasing trend, returning to follow the AMO trend in 2011 (Figure 8B).

We decomposed the average incident energy flux on the coast into the four main quadrants and related them to the AMO index variation from 1979 to 2019 (Figure 9). All quadrants followed the general trend of AMO variation, with a correlation coefficient (95% significance level) for the ENE of R = 0.89; for the ESE of R = 0.91; for the SSE of R = 0.97; and for the SSW of R = 0.86. According to Odériz et al. (2020), the correlation values between the WEF and AMO are considered very strong (R> 0.75). The largest range of WEFm variation was associated with the SSW quadrant, as shown in Figure 9D.

DISCUSSION

WEF TRENDS AND BREAKPOINTS

As shown in Table 3 and Figure 3, the general WEFm presented a significantly positive linear trend over the entire analyzed period (between
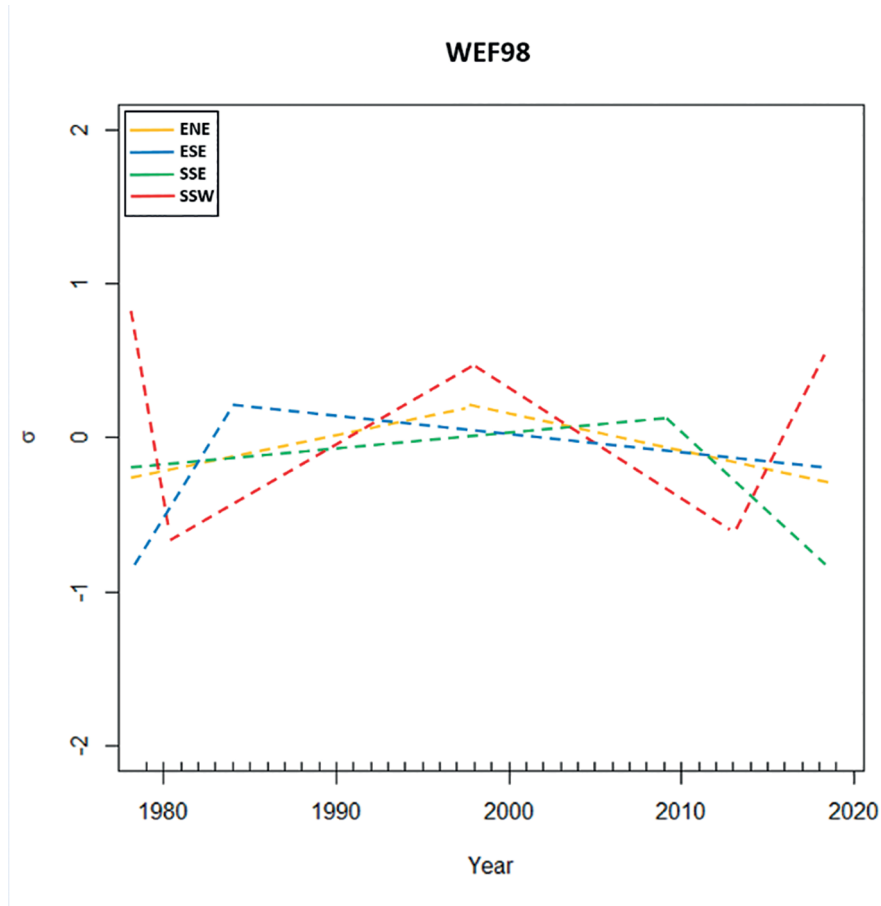
WEF98

Figure 7. WEF98 variation per quadrant. Segmented lines indicate subperiods without significant variations. WEF98= extreme wave energy flux (98th percentile).
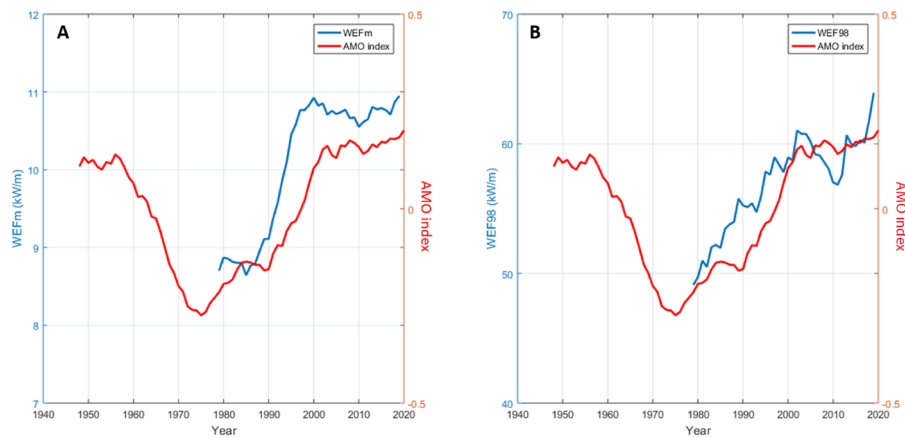

Figure 8. Comparison between the AMO index (red line), 10-year running mean WEFm (blue line, A) and 10-year running mean WEF98 (blue line, B). AMO= Atlantic Multidecadal Oscillation; WEFm = mean wave energy flux; WEF98= extreme wave energy flux (98th percentile).

1979 and 2019) at an increase rate of 0.063 kW/m/year, which was equivalent to an annual increase of 0.63% and indicates more energy transference

from the atmosphere to the ocean surface motion- This value is similar to the 0.58% found by Reguero et al. (2019) as a mean of annual increase rate
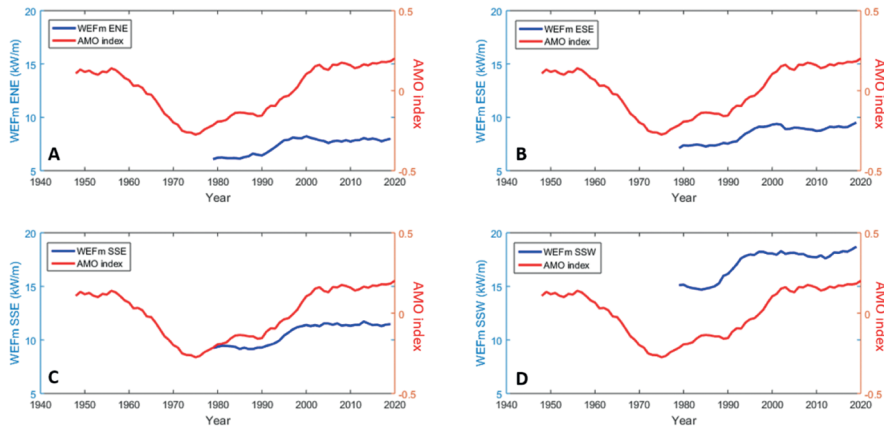
Figure 9. Comparison between the AMO index (red line) and 10-year running mean WEFm values per quadrant (blue lines). AMO= Atlantic Multidecadal Oscillation; WEF = mean wave energy flux.

between 1948 and 2008 to the Southern Ocean (between 40 and 80°S), which besides being that is the most energetic oceanic basin and dominates the other oceans in terms of wave power has a great influence as a generation area on the wave characteristics of our analyzed region. To the same period, according to these authors the global mean WEFm has increased 0,47% per year. The general extreme condition (WEF98) also presented a significantly positive linear trend over the entire analyzed period, with an increase rate of 0.17 kW/m/year, that corresponds to an annual increase of 0.29%. (Table 3 and Figure 3). The results found related with WEFm and WEF98 are in line with global tendencies. According to Mentaschi et al. (2017), the WEF along coasts worldwide is projected to increase significantly by the end of the century, mainly in the Southern Hemisphere. Semedo et al. (2013) found that changes in the wave climate toward the end of the twenty-first century are small to moderate, with the largest signals being a poleward shift in the annual mean significant wave heights in the midlatitudes of both hemispheres, which is more pronounced in the Southern Hemisphere and most likely associated with a corresponding shift in midlatitude storm tracks.

The studies by Reguero et al. (2013) and Alonso and Solari (2021) indicated that the WEF on the West Atlantic coast is undergoing a clockwise rotational trend. These changes are probably related to the trend of rotating toward the poles detected in extratropical storm activity (Meehl et

al., 2007), which indicates more storm activity at high latitudes that is more pronounced in the Southern Hemisphere (Bengtsson et al., 2006). In fact, by applying the Muggeo method, we observed in Figure. 6 that the swell coming from the southernmost quadrants (SSW and SSE) were the first to show a significant upward trend in WEFm between 1986-1992 and 1989-1999 respectively, while the ESE swell showed between 1997-2013 the longest range of a subperiod with a significant negative trend.

Rotating southward in the clockwise direction, we observed that waves coming from the ESE (2013-2019), SSE (1989-1999) and SSW (1986-1992) quadrants showed an increasing range scale in significant positive trends associated with general WEFm (Fig. 6) and that only the southern quadrants (SSE and SSW) were responsible for inducing significant positive trends in WEFm (Fig. 4, subperiod II). A relevant factor is associated with the fact that, by decomposing Figure 4 into 4 quadrants of wave incidence we observed that the segmented WEFm trends (Fig. 4) are primarily driven by the swell coming from SSW and secondarily by waves from SSE (Fig. 6).This trends coupled with the fact that the swell from southern quadrants are the most energetic (Table 4) suggests that these waves are probably mainly responsible for the increasing trend of thegeneral WEFm (Figure 3), since as can be seen in Table 5 the SSE and SSW quadrants have the highest annual increment rates associated with WEFm, 0.073 kW/m/year and 0.094 kW/m/year respectively. This scenario is of considerable relevance since swells

generated in the Southern Ocean are projected to be more energetic in the coming years (Young et al. 2011; Babanin et al. 2019) and, in the western South Atlantic Ocean, SW swells are strongly influenced by winds from low latitudes generated by the Migratory Polar Anticyclone (APM), which is responsible for the generation of storms that can suddenly impact the coastline when they reach the continent (Calliari et al. 1998; Parise et al. 2009; Machado et al. 2010).

Although the subperiods associated with WEF98 show no significant trend (Fig. 5), their inflection points and subperiods also resemble the behavior of the WEF98 subperiods associated with the SSE and SSW quadrants. However, it is worth noting that in a linear analysis as evidenced in Figure 3, WEF98 shows a significant growth trend at a rate of 0.17 kW/m/year equaling 0.29% per year (Table 3). These results are relevant since, according to some authors, this trend in extreme wave conditions may intensify in the coming years. Mentaschi et al. (2017) conducted a comprehensive modeling analysis to identify future global trends in extreme wave energy flux along coastlines in the 21st century under a high emission pathway (RCP 8.5 - IPCC) and identified that the WEF increment translates into considerable changes in the recurrence frequency of extreme events, which is projected double in many areas, especially in the Southern Hemisphere where an increase in the extreme WEF is projected until 2100 implying an intensification of coastal erosion and wave-induced impacts. Corroborating these results and also under the RCP 8.5 scenario, Meucci et al. (2020) project an increase by up to 20% in the 100-year significant wave height of the Southern and South Atlantic Oceans by 2100, which would have the potential to increase the extreme conditions of WEF of these regions.

WEF VARIATIONS AND THE AMO INDEX

Wave conditions are expected to respond to climatic variations. In recent decades, for example, positive correlations were obtained between sea surface temperatures in the Tropical and North Atlantic and wave power in the southern extratropics, suggesting an intensification of energy transfer from wind fields into wave generation in these regions as a result of warming trends (Reguero et al. 2019; Silva et al. 2020). Consequently, the WEF variability reflects changes in the predominant wave-generating atmospheric systems, which are normally caused by large-scale climatic drivers (Hemer et al. 2010, Reguero et al. 2019, Silva et al. 2020). Globally, Mentaschi et al. (2017) and Odériz et al. (2020) showed that the most significant long-term WEF trends can be explained by the intensification of teleconnection patterns such as the Antarctic Oscillation, El Niño–Southern Oscillation, North Atlantic Oscillation and Atlantic Multidecadal Oscillation.

As demonstrated by Young et al. (2011) and Yang et al. (2020), it is highly likely that long-term oscillations, such as the AMO, significantly influence the global ocean wind and wave climate since global-scale multidecadal SST variability could be driven by the AMO through atmospheric teleconnections and atmosphere–ocean coupling processes. According to Alexander et al. (2014) and Odériz et al. (2020), the Atlantic Ocean exhibits variability over a wide range of temporal and spatial scales but has pronounced variability at decadal and multidecadal timescales, playing a key role in the multidecadal oscillation of global SST (Yang et al. 2020).

Through calculation of correlation between WEF and climate indices Odériz et al. (2020) indicated that the WEF that reaches both Mexican coasts is influenced by the AMO on multidecadal timescales, once the AMO shows a regionally consistent wave climate response of moderate positive correlation on the Yucatan Peninsula and entire Pacific coast for WEF. Thus, according with these authors not only the Atlantic but also the Pacific Ocean may have the long-term variability of WEF driven by AMO, wich positive (negative) phases drives an increase (decrease) in wave power. Kayano et al. (2019) show that low-level extratropical cyclones in the South Atlantic are modulated by AMO-related SST anomalies, with positive anomalies affecting the cyclone trajectories and meridional SST gradients that influence the baroclinicity of long waves, which in turn enters the energy Lorenz cycle. This fact is of great importance for the region, once extratropical cyclones are known to generate extreme significant wave height values and consequentely improving

WEF at the ocean surface in the western South Atlantic (Sasaki et al. 2021). At atmospheric levels in both AMO phases, the highest baroclinic and barotropic energy conversion values occur along the 30°–50° and 20°–50°S bands, with the largest cyclone local counts in the southwestern Atlantic, specifically on the Argentina, Uruguay and southern Brazil coasts (Sinclair 1995, 1997; Kayano et al. 2019). According to Kayano et al. (op. cit.), the kinetic energy in warm AMO phases surpasses that in cold AMO phases; thus, the considerably more energetic low-level cyclones lead to higher energy conversion terms in warm phases than in cold phases, inducing more energetic cyclones with high potential to transfer energy from the atmosphere to the ocean and increase the WEF during warm phases.

As documented by Escobar et al. (2004), Bischoff (2005) and Ortega et al. (2013), SE storms were at a minimum during the downward phase of the AMO curve and increased thereafter, especially at the beginning of the warm AMO phase. Corroborating these results, we observed that the WEFm curves associated with SE quadrants present, in addition to the larger ones, a very strong correlation with the AMO curve (SSE, R = 0.97, Figure 9C and ESE, R = 0.91, Figure 9B), where such curves develop covariant behavior from the cold until warm phases of AMO.. In this sense, in the western South Atlantic Ocean and along the rising phase of the AMO curve, D'Onofrio et al. (2008) showed that the decadal average frequency and duration of positive surges have increased, and Codignotto et al. (2012) described an increment in the frequency and height of wind waves propagating from the south. Additionally, related to variations in AMO phases, Wang et al. (2008) described that between 1854–2006, Atlantic hurricanes presented major and minor activities during the warm and cold AMO phases, respectively, suggesting that multidecadal variability in oceanic temperatures may be responsible for multidecadal variation in Atlantic hurricane activity. These authors also showed that Atlantic tropical cyclone activities have largely increased in frequency and intensity since the late 1980s. Reinforcing these results, we observed that during the transition period from the cold to warm AMO phase between the late 1980s and 1990s, the WEF98 and mainly the WEFm curve covary with the AMO curve (Figure 8A and B), exhibiting a growing trend. In the same period, the WEFm associated with the SSE and SSW quadrants also showed a significant growth trends (Figure 6) and similar behavior to that of the AMO curve (Figure 9C and D). Since that the driving mechanism of the AMO is related to variability in the oceanic thermohaline circulation (Knight et al., 2005) involving fluctuations of the Atlantic meridional overturning circulation (AMOC) (Delworth and Mann, 2000; Knight et al., 2005; Dijkstra et al., 2006) and on a multidecadal scale the Southern Ocean is first to show changes in this circulation patters (Crowley and Kim 1993), Kayano et al. 2019 demonstrated that during the AMO warm phase the region between 40°-70°S latitudes, which is exactly where the most energetic waves (SSE and SSW) come from, presented strong SST anomalies and inverse temperature patterns in relation to the cold phase. On the whole, spatiotemporal SST gradients are known to be a critical driver in ocean-atmosphere teleconnections and influence wind patterns and consequently WEF along the oceans (Reguero et al. 2019). Thus, it is to be expected that eventual changes in SST patterns in the Southern Ocean eventually induced by AMO influence the variability of the WEF in our study area. As can be seen in Figure 6 the SSW quadrant swell was the first to show a significant trend of increasing WEFm (late 1980s) and subsequently the SSE swell also started a significant growth phase. Such swells have their origin related to the higher latitudes, reflecting primarily the changes in the Southern Ocean eventually induced by the AMO during its transition from the cold phase to the warm phase (Fig. 8, late 1980s and 1990s; Fig.4, subperiod II). This kind of behavior is in agreement with other studies in the western South Atlantic Ocean, which also found a link between the recent warm phase of the AMO and physical environmental changes (Bischoff 2005 and Ortega et al. 2013), reinforcing the evidence of a correlation between the warm AMO phases and the energy intensification associated with meteo-oceanographic elements.

Increases in wave height primarily occur from increased surface wind energy, but the global wind

patterns change in response to spatiotemporal SST variations (Inatsu et al. 2002; Bengtsson et al. 2006). For this reason, to understand WEF trend changes in the southern Brazil we studied their correlations with the long-term tendencies of the AMO index, a SST-based climate index Although we focused on this singular mode (AMO), wave generation and the wave climate in the South Atlantic Ocean results from variability in a number of atmospheric patterns, large-scale drivers and teleconnections, many of which remain understudied compared with those in other global regions (Reguero et al. 2013; Reguero et al. 2019; Silva et al. 2020). Although the relationship between the AMO and WEF does not explain the interannual variability, it seems to have a profound effect on long-term WEF variations and trends. As evidence for this statement, the long-term trend computed with the 10-year filtered WEFm and WEF98 resulted in very strong correlations with the AMO curve. These results suggest that the trends observed in WEFm and WEF98 curves presented in this study likely represent the result of a long-term transition from a cold (negative) to warm (positive) AMO phase, which could modulate the long-term component of the interannual WEF98 and mainly the WEFm in the western South Atlantic. This relationship between the AMO and the western South Atlantic Ocean WEF has not been previously described. Since the AMO is still in its warm phase, it is expected that the WEF in coastal regions adjacent to the western South Atlantic Ocean will remain high in the next few years. This requires planning regarding the coastal management of these areas to avoid and mitigate potential wave-induced impacts attributed to the high flux of energy from the adjacent ocean. Further research should be performed, preferably using longer wave time series to identify WEF breakpoints and to investigate the effect of a full cycle of the AMO index on the wave characteristics.

CONCLUSION

This study investigated historical breakpoints and trends in wave energy flux (WEF) over 41 years in southern Brazil. The comparison between ERA-5 data and measurements from a waverider showed overall high agreement for wave parameters, proving ERA-5 to be a very useful database for long-term analyses. The WEFm and WEF98 presented a significantly positive linear trends between 1979 and 2019, with an increasing rates of 0.063 and 0.17 kW/m/year corresponding to 0.63 and 0.29% per year respectively.. Among all quadrants, the incident waves of the SSE and SSW quadrants presented the highest values of both the WEFm and WEF98, and by the Muggeo method, it was possible to identify that the WEFm associated with these quadrants seems to be related to subperiods that present positive advancing trends in the incremental general WEFm. The present results highlight that the general long-term WEFm and WEF98 signals are very strongly correlated with the AMO index (correlation coefficient = 0.92 and 0.89, respectively) and, consequently, suggest that the identified positive trends in the WEFm and WEF98 are likely related to the transition of cold to warm AMO phase in the western South Atlantic Ocean. We also determined that the WEFm curves of all quadrants follow the general trend of the AMO curve variation; however, the WEFm curve from the SSE quadrant has a greater correlation. Given that the AMO is still in its warm phase and that we have observed a very strong correlation between it and the WEF behavior, high WEF values are still expected in the western South Atlantic Ocean in the coming years. These incremental trends reinforce the need to develop efficient coastal management policies to adapt mainly regions with low declivity and chiefly mitigate potential impacts related to erosion and flooding processes. Along with coastal planning, further investigation should be performed to explore the relationship between WEF characteristics and full cycles of the AMO, as well as other climatic indices with different periodicities.

ACKNOWLEDGMENTS

AUTHOR CONTRIBUTIONS

N.Z.M.: Conceptualization, Methodology, Formal analysis, Investigation, Writing - original draft, Writing - review & editing

L.P.A.: Conceptualization, Methodology, Formal analysis, Investigation, Writing - review & editing

L.E.: Methodology, Formal analysis, Investigation, Writing - review & editing

J.L.N.: Formal analysis, Investigation, Writing - review & editing

L.C.: Formal analysis, Investigation, Writing - review & editing

REFERENCES

ALEXANDER, M. A., KILBOURNE, K. H. & NYE, J. A. 2014. Climate variability during warm and cold phases of the Atlantic Multidecadal Oscillation (AMO) 1871-2008. *Journal of Marine Systems*, 133, 14-26, DOI: https://doi.org/10.1016/j.jmarsys.2013.07.017

ALHEIT, J., LICANDRO, P., COOMBS, S., GARCIA, A., GIRÁLDEZ, A., SANTAMARÍA, M. T. G., SLOTTE, A. & TSIKLIRAS, A. C. 2014. Atlantic Multidecadal Oscillation (AMO) modulates dynamics of small pelagic fishes and ecosystem regime shifts in the eastern North and Central Atlantic. *Journal of Marine Systems*, 133, 88-102, DOI: https://doi.org/10.1016/j.jmarsys.2014.02.005

ALMEIDA, L. P., FERREIRA, Ó., VOUSDOUKAS, M. I. & DODET, G. 2011. Historical variation and trends in storminess along the Portuguese South Coast. *Natural Hazards and Earth System Science*, 11(9), 2407-2417, DOI: https://doi.org/10.5194/nhess-11-2407-2011

ANTOLÍNEZ, J. A. A., MENDEZ, F. J., CAMUS, P., VITOUSEK, S., GONZÁLEZ, E. M., RUGGIERO, P. & BARNARD, P. 2016. A multiscale climate emulator for long-term morphodynamics (MUSCLE- morpho). *Journal of Geophysical Research-Oceans*, 121(1), 775-791, DOI: https://doi.org/10.1002/2015JC011107

BABANIN, A. V., ROGERS, W. E., CAMARGO, R., DOBLE, M., DURRANT, T., FILCHUCK, K., EWANS, K., HEMER, M., JANSSEN, T., KELLY-GERREYN, B., MACHUTCHON, K., MCCOMB, P., QIAO, F., SCHULZ, E., SKVORTSOV, A., VICHI, M., VIOLANTE-CARVALHO, N., WANG, D., WASEDA, T., WILLIAMNS, G. & YOUNG, I. R. 2019. Waves and swells in high wind and extreme fetches, measurements in the southern ocean. *Frontiers in Marine Science*, 6, 361, DOI: https://doi.org/10.3389/fmars.2019.00361

BENGTSSON, L., HODGES, K. & ROECKNER, E. 2006. Storm tracks and climate change. *Journal of Climate,* 19, 3518-3543.

BIASTOCH, A., DURGADOO, J. V., MORRISON, A. K., VAN SEBILLE, E., WEIJER, W. & GRIFFIES, S. M. 2015. Atlantic multi-decadal oscillation covaries with Agulhas leakage. *Nature Communications*, 6, 10082, DOI: https://doi.org/10.1038/ncomms10082

BISCHOFF, S. 2005. Sudestadas. *In:* BARROS, V., MENÉNDEZ, A. & NAGY, G. (eds.). *El Cambio Climatico en el Rio de la Plata*. Buenos Aires: Universidad de Buenos Aires, pp. 53-67.

CALLIARI, L. J. & KLEIN, A. H. F. 1993. Características morfodinâmicas e sedimentológicas das praias oceânicas entre Rio Grande e Chuí, RS. *Pesquisas em Geociências,* 20(1), 48-56.

CALLIARI, L. J., TOZZI, H. A. M. & KLEIN, A. H. F. 1998. Beach morphology and coastline erosion associated with storm surges in Southern Brazil - Rio Grande to Chuí, RS. *Anais da Academia Brasileira de Ciência*, 70(2), 175-188.

CHIESSI, C. M., MULITZA, S., PÄTZOLD, J., WEFER, G. & MARENGO, J. A. 2009. Possible impact of the Atlantic Multidecadal Oscillation on the South American summer monsoon. *Geophysical Research Letters*, 36(21), 1-5, DOI: https://doi.org/10.1029/2009GL039914

CODIGNOTTO, J. O., DRAGANI, W. C., MARTIN, P. B., SIMIONATO, C. G., MEDINA, R. A. & ALONSO, G. 2012. Wind-wave climate change and increasing erosion in the outer Río de la Plata, Argentina. *Continental Shelf Research*, 38, 110-116, DOI: https://doi.org/10.1016/j.csr.2012.03.013

COPERNICUS CLIMATE CHANGE SERVICE (CCCS). 2017. *ERA5: Fifth generation of ECMWF atmospheric reanalyses of the global climate*. Brussels: Copernicus Climate Change Service Climate Data Store (CDS).

CROWLEY, T. J. & KIM, K. Y. 1993. Towards development of a strategy for determining the origin of decadal-centennial scale climate variability. *Quaternary Science Reviews*, 12(6), 375-385, DOI: https://doi.org/10.1016/S0277-3791(05)80003-4

DAVIES, J. L. 1964. A morphogenic approach to world shorelines. *Geomorphology*, 8(5), 27-142.

DEE, D. P., UPPALA, S. M., SIMMONS, A. J., BERRISFORD, P., POLI, P., KOBAYASHI, S., ANDRAE, U., BALMASEDA, M. A., BALSAMO, G., BAUER, P., BECHTOLD, P., BELJAARS, A. C. M., VAN DE BERG, L., BIDLOT, J., BORMANN, N., DELSOL, C., DRAGANI, R., FUENTES, M., GEER, A. J., HAIMBERGER, L., HEALY, S. B., HERSBACH, H., HOLM, E. V., ISAKSEN, L., K´ALLBERG, P., KOHLER, M., MATRICARDI, M., MCNALLY, A. P., MONGE-SANZ, B. M., MORCRETTE, J. J., PARK, B. K., PEUBEY, C., ROSNAY, P., TAVOLATO, C., THEPAUT, J. N. & VITART, F. 2011. The ERA-Interim reanalysis: configuration and performance of the data assimilation system. *Quaternary Journal of the Royal Meteorological Society*, 137(656), 553-597, DOI: https://doi.org/10.1002/qj.828

DE LEO, F., BESIO, G. & MENTASCHI, L. 2021. Trends and variability of ocean waves under RCP8.5 emission scenario in the Mediterranean Sea. *Ocean Dynamics*, 71, 97-117, DOI: https://doi.org/10.1007/s10236-020-01419-8

DELWORTH, T. L. & MANN, M. E. 2000. Observed and simulated multidecadal variability in the Northern Hemisphere. *Climate Dynamics*, 16, 661-676, DOI: https://doi.org/10.1007/s003820000075

DIJKSTRA, H. A., TE RAA, L., SCHMEITS, M. & GERRITS, J. 2006. On the physics of the Atlantic Multidecadal Oscillation. *Ocean Dynamics*, 56, 36-50, DOI: https://doi.org/10.1007/s10236-005-0043-0

DODET, G., BERTIN, X. & TABORDA, R. 2010. Wave climate variability in the North-East Atlantic Ocean over the last six decades. *Ocean Modelling*, 31(3), 120-131.

D'ONOFRIO, E. E., FIORE, M. E. & POUSA, J. L. 2008. Changes in the regime of storm surges at Buenos Aires, Argentina. *Journal of Coastal Research*, 24(1A), 260-265.

ENFIELD, D. B., MESTAS-NUÑEZ, A. M. & TRIMBLE, P. J. 2001. The Atlantic Multidecadal Oscillation and its relationship to rainfall and river flows in the continental U.S. *Geophysical Research Letters*, 28(10), 2077-2080, DOI: https://doi.org/10.1029/2000GL012745

ESCOBAR, G., VARGAS, W. & BISCHOFF, S. 2004. Wind tides in the Rio de la Plata estuary: meteorological conditions. *International Journal of Climatology*, 24(9), 1159-1169.

FRAJKA-WILLIAMS, E., BEAULIEU, C. & DUCHEZ, A. 2017. Emerging negative Atlantic Multidecadal Oscillation index in spite of warm subtropics. *Scientific Reports*, 7(1), 11224, DOI: https://doi.org/10.1038/s41598-017-11046-x

FURG (Universidade Federal do Rio Grande). *Rede Ondas* [online]. Porto Alegre: FURG (Universidade Federal do Rio Grande). Avaliable at: www.redeondas.furg.br [Accessed: YEAR Mo DAY].

GARNER, A. J., MANN, M. E., EMANUEL, K. A., KOPP, R. E., LIN, N., ALLEY, R. B. & POLLARD, D. 2017. Impact of climate change on New York City's coastal flood hazard: Increasing flood heights from the preindustrial to 2300 CE. *Proceedings of the National Academy of Sciences of the United States of America,* 114(45), 11861-11866, DOI: https://doi.org/10.1073/pnas.1703568114

GODOLPHIM, M. F. 1976. *Geologia do Holoceno Costeiro do Município do Rio Grande, RS*. MSc. Porto Alegre: UFRGS (Universidade Federal do Rio Grande do Sul) - Instituto de Geociências.

GOLDENBERG, S. B., LANDSEA, C. W., MESTAS-NUNEZ, A. M. & GRAY, W. M. 2001. The recent increase in Atlantic hurricane activity: causes and implications. *Science*, 293(5529), 474-479, DOI: https://doi.org/10.1126/science.1060040

GONZALES, M., NICOLODI, J. L., GUTIÉRREZ, O. Q., LOSADA, V. C. & HERMOSA, A. E. 2016. Brazilian coastal processes: wind, wave climate and sea level. *In:* SHORT, A. D. & KLEIN, A. H. F. (orgs.). *Brazilian beach systems.* Switzerland: Springer International Publishing, v. 17, pp. 37-66.

HARLEY, M. D., TURNER, I. L., SHORT, A. D. & RANASINGHE, R. 2010. Interannual variability and controls of the Sydney wave climate. *International Journal of Climatology*, 30(9), 1322-1335.

HEMER, M. A., CHURCH, J. A. & HUNTER, J. R. 2010. Variability and trends in the directional wave climate of the Southern Hemisphere. *International Journal of Climatology*, 30(4), 475-491, DOI: https://doi.org/10.1002/joc.1900

HEMER, M. A., CHURCH, J. A., SWAIL, V. & WANG, X. 2006. Coordinated global wave climate projections. *Atmosphere-Ocean Interactions,* 2, 185-218.

HERSBACH, H., BELL, B., BERRISFORD, P., HIRAHARA, S., HORÁNYI, A., MUÑOZ-SABATER, J. & THÉPAUT, J. N. 2020. The ERA5 global reanalysis. *Quarterly Journal of the Royal Meteorological Society*, 146(730), 1999-2049, DOI: https://doi.org/10.1002/qj.3803

HOSKINS, B. J. & HODGES, K. I. A. 2005. New Perspective on Sourthern Hemisphere Storm Tracks. *Journal of Climate*, 18, 4108-4129.

HURREL, H., KUSHNIR, Y., OTTERSEN, G. & VISBECK, M. 2003. An overview of the North Atlantic oscillation. The North Atlantic Oscillation: climatic significance and environmental impact. *Geophysical Monograph Series*, 134, 1-35.

KAYANO, M. T., ROSA, M. B., RAO, V. B., ANDREOLI, R. V. & SOUZA, R. A. F. 2019. Relations of the low-level extratropical cyclones in the southeast Pacific and South Atlantic to the Atlantic multidecadal oscillation. *Journal of Climate*, 32(14), 4167-4178, DOI: https://doi.org/10.1175/JCLI-D-18-0564.1

KERR, R. A. 2000. A North Atlantic climate pacemaker for the centuries. *Science*, 288(5473), 1984-1986, DOI: https://doi.org/10.1126/science.288.5473.1984

KING, C. A. M. 1972. *Beaches and coasts*. London: Edward Arnold.

KNIGHT, J. R., ALLAN, R. J., FOLLAND, C. K., VELLINGA, M. & MANN, M. E. 2005. A signature of persistent natural thermohaline circulation cycles in observed climate. *Geophysical Research Letters*, 32, L20708, DOI: https://doi.org/10.1029/2005GL024233

KNIGHT, J. R., FOLLAND, C. K. & SCAIFE, A. A. 2006. Climate impacts of the Atlantic Multidecadal Oscillation. *Geophysical Research Letters,* 33(17), L17706, DOI: https://doi.org/10.1029/2006GL026242

KRAVTSOV, S. V. & SPANNAGLE, C. 2008. Multi-decadal climate variability in observed and modeled surface temperature. *Journal of Climate*, 21(5), 1104-1121, DOI: https://doi.org/10.1175/2007JCLI1874.1

KUSHNIR, Y., CARDONE, V. J., GREENWOOD, J. G. & CANE, M. A. 1997. The recent increase in North Atlantic wave heights. *Journal of Climate*, 10, 2107-2113.

LATIF, M. 2013. The Ocean's role in modeling and predicting decadal climate variations. *In:* SIEDLER, G., GRIFFIES, S. M., GOULD, J. & CHURCH, J. A. (eds.). *International geophysics*. London: Academic Press, v. 103, pp. 645-665.

LYU, K. & YU, J. Y. 2017. Climate impacts of the Atlantic Multidecadal Oscillation simulated in the CMIP5 models: a re-evaluation based on a revised index. *Geophysical Research Letters*, 44(8), 3867-3876, DOI: https://doi.org/10.1002/2017GL072681

MACHADO, A. A., CALLIARI, L. J., MELO, E. & KLEIN, A. H. F. 2010. Historical assessment of extreme coastal sea state conditions in southern Brazil and their relation to erosion episodes [online]. *Pan American Journal of Aquatic Sciences*, 5(2), 277-286. Available at: http://www.panamjas.org/pdf_artigos/PANAMJAS_5(2)_277-286.pdf [Accessed: YEAR Mo DAY].

MAIA, N. Z., CALLIARI, L. J. & NICOLODI, J. L. 2016. Analytical model of sea level elevation during a storm: Support for coastal flood risk assessment associated with cyclone passage. *Continental Shelf Research*, 124, 23-34, DOI: https://doi.org/10.1016/j.csr.2016.04.012

MARSHALL, A. G., HEMER, M. A., HENDON, H. H. & MCINNES, K. L. 2018. Southern annular mode impacts on global ocean surface waves. *Ocean Modelling*, 129, 58-74, DOI: https://doi.org/10.1016/j.ocemod.2018.07.007

MCCABE, G. J., PALECKI, M. A. & BETANCOURT, J. L. 2004. Pacific and Atlantic Ocean influences on multidecadal drought frequency in the United States. *Proceedings of the National Academy of Sciences of the United States of America*, 101(12), 4136-4141, DOI: https://doi.org/10.1073/pnas.0306738101

MEEHL, G., STOCKER, T., COLLINS, W., FIEDLINGSTEIN, P., GAYE, A., GREGORY, KITOH, A., KNUTTI, R., MURPHY, J., NODA, A., RPER, S., WATTERSON, I., WEAVER, A. & ZHAO, Z. 2007. *Climate change 2007: the physical science basis. Contribution of Working Group I to the Fourth Assessment Report of the Intergovernmental Panel on Climate Change, Chapter Global Climate Projections*. Cambridge: Cambridge University Press.

MENTASCHI, L., VOUSDOUKAS, M. I., VOUKOUVALAS, E., DOSIO, A. & FEYEN, L. 2017. Global changes of extreme coastal wave energy fluxes triggered by intensified teleconnection patterns. *Geophysical Research Letters,* 44(5), 2416-2426.

MORI, N., YASUDA, T., MASE, H., TOM, T. & OKU, Y. 2010. Projection of extreme wave climate under global warming. *Hydrological Research Letters,* 4, 14-19.

MORIM, J., HEMER, M., WANG, X. L., CARTWRIGHT, N., TRENHAM, C., SEMEDO, A., YOUNG, I., BRICHENO, L., CAMUS, P., CASAS-PRAT, M., ERIKSON, L., MENTASCHI, L., MORI, N., SHIMURA, T., TIMMERMANS, B., AARNES, O., BREIVIK, O., BEHRENS, A., DOBRYIN, M., MENENDEZ, M., STANEVA, J., WEHNER, M., WOLF, J., KAMRANZAD, B., WEBB, A., STOPA, J. & ANDUTTA, F. 2019. Robustness and uncertainties in global multivariate wind-wave climate projections. *Nature Climate Change*, 9(9), 711-718, DOI: https://doi.org/10.1038/s41558-019-0542-5

MOTTA, V. F. 1969. Relatório-diagnóstico sobre a melhoria e o aprofundamento do acesso pela barra de Rio Grande. MSc. Porto Alegre: UFRGS (Universidade Federal do Rio Grande do Sul) - Instituto de Pesquisas Hidráulicas.

MUGGEO, V. M. 2003. Estimating regression models with unknown break-points. *Statistics in Medicine*, 22(19), 3055-3071.

NOAA (National Oceanic and Atmospheric Administration). 2001. *Climate Timeseries – AMO (Atlantic Multidecadal Oscillation) index* [online]. Boulder: NOOA. Available at: https://psl.noaa.gov/data/timeseries/AMO/ [Accessed: 2020 Apr 04].

ODÉRIZ, I., SILVA, R., MORTLOCK, T. R. & MENDOZA, E. 2020. Climate drivers of directional wave power on the Mexican coast. *Ocean Dynamics*, 70(9), 1253-1265, DOI: https://doi.org/10.1007/s10236-020-01387-z

OLIVEIRA, B. A., SOBRAL, F., FETTER, A. & MENDEZ, F. J. 2019. A high-resolution wave hindcast off Santa Catarina (Brazil) for identifying wave climate variability. *Regional Studies in Marine Science*, 32, 100834.

OLIVEIRA, U. R., SIMÕES, R. S., CALLIARI, L. J. & GAUTÉRIO, B. C. 2019. Erosão de dunas sob ação de um evento extremo de alta energia de ondas na costa central e sul do Rio Grande do Sul, Brasil. *Revista Brasileira de Geomorfologia*, 20(1), 1-22, DOI: http://dx.doi.org/10.20502/rbg.v20i1.1352

O'REILLY, C. H., WOOLLINGS, T. & ZANNA, L. 2017. The dynamical influence of the Atlantic multidecadal oscillation on continental climate. *Journal of Climate*, 30(18), 7213-7230, DOI: https://doi.org/10.1175/JCLI-D-16-0345.1

ORTEGA, L., CELENTANO, E., FINKL, C. & DEFEO, O. 2013. Effects of climate variability on the morphodynamics of Uruguayan sandy beaches. *Journal of Coastal Research*, 29(4), 747-755.

PARISE, C. K., CALLIARI, L. J. & KRUSCHE, N. 2009. Extreme storm surges in the south of Brazil: atmospheric conditions and shore erosion. *Brazilian Journal of Oceanography*, 57(3), 175-188.

PEZZI, L. P., SOUZA, R. B. & QUADRO, M. F. L. 2016. Uma revisão dos processos de interação oceano-atmosfera em regiões de intenso gradiente termal do oceano Atlântico Sul baseada em dados observacionais. *Revista Brasileira de Meteorologia*, 31(4), 428-453, DOI: https://doi.org/10.1590/0102-778631231420150032

PIANCA, C., MAZZINI, P. L. & SIEGLE, E. 2010. Brazilian offshore wave climate based on NWW3 reanalysis. *Brazilian Journal of Oceanography*, 58(1), 53-70.

QIAN, C., YU, J. Y. & CHEN, G. 2014. Decadal summer drought frequency in China: the increasing influence of the Atlantic multi-decadal oscillation. *Environmental Research Letters*, 9(12), 124004, DOI: https://doi.org/10.1088/1748-9326/9/12/124004

RASMUSSEN, D. J., BITTERMANN, K., BUCHANAN, M. K., KULP, S., STRAUSS, B. H., KOPP, R. E. & OPPENHEIMER, M. 2018. Extreme sea level implications of 1.5 °C, 2.0 °C, and 2.5 °C temperature stabilization targets in the 21st and 22nd century. *Environmental Research Letters*, 13, 034040.

REGUERO, B. G., LOSADA, I. J. & MENDEZ, F. J. 2019. A recent increase in global wave power as a consequence of oceanic warming. *Nature Communications*, 205, 1-14.

REGUERO, B. G., MÉNDEZ, F. J. & LOSADA, I. J. 2013. Variability of multivariate wave climate in Latin America and the Caribbean. *Global and Planetary Change,* 100, 70-84.

SEMEDO, A., SUSELIJ, K., RUTGERSSON, A. & STERL, A. 2011. A global view on the wind sea and swell climate and variability from ERA-40. *Journal of Climate,* 24(5), 1461-1479.

SEMEDO, A., WEISSE, R., BEHRENS, A., STERL, A., BENGTSSON, L. & GÜNTHER, H. 2013. Projection of global wave climate change toward the end of the twenty-first century. *Journal of Climate*, 26(21), 8269-8288, DOI: https://doi.org/10.1175/JCLI-D-12-00658.1

SILVA, A. P., KLEIN, A. H. F., FETTER-FILHO, A. F. H., HEIN, C. J., MÉNDEZ, F. J., BROGGIO, M. F. & DALINGHAUS, C. 2020. Climate-induced variability in South Atlantic wave direction over the past three millennia. *Scientific Reports*, 10, 18553, DOI: https://doi.org/10.1038/s41598-020-75265-5

SINCLAIR, M. R. 1995. A climatology of cyclogenesis for the Southern Hemisphere. *Monthly Weather Review*, 123, 1601-1619.

SINCLAIR, M. R. 1997. Objective identification of cyclones and their circulation intensity, and climatology. *Weather and Forecasting*, 12(3), 595-612.

SUN, C., LI, J. & ZHAO, S. 2015. Remote influence of Atlantic multidecadal variability on Siberian warm season precipitation. *Scientific Reports*, DOI: https://doi.org/10.1038/srep16853

SWAIL, V. R., CECCACCI, E. A. & COX, A. T. 2000. The AES40 north Atlantic wave reanalysis validation and climate assessment. *In: 6th International Workshop on Wave Hindcasting and Forecasting (WWHF)*. Monterey, California, USA, 2000 Nov 6-10. Monterey: WWHF, pp. 1-17.

THE WAMDI GROUP. 1988. The WAM Model - A Third Generation Ocean Wave Prediction Model. *Journal of Physical Oceanography*, 18(12), 1775-1810.

THOMPSON, D. & WALLACE, J. M. 1998. The Arctic Oscillation signature in the wintertime geopotential height and temperature fields. *Geophysical Research Letters*, 25(9), 1297-1300.

TIMMERMANN, A., OKUMURA, Y., AN, S. I., CLEMENT, A., DONG, B., GUILYARDI, E., HU, A., JUNCLAUS, J. H., RENOLD, M., STOCKER, T. F., STOUFFER, R. J., SUTTON, R., XIE, S. P. & YIN, J. 2007. The influence of a weakening of the Atlantic meridional overturning circulation on ENSO. *Journal of Climate*, 20(19), 4899-4919, DOI: https://doi.org/10.1175/JCLI4283.1

TOMAZELLI, L. J. & VILLWOCK, J. A. 1992. Algumas Considerações sobre o Ambiente Praial e a Deriva Litorânea de Sedimentos ao Longo do Litoral Norte do Rio Grande do Sul, Brasil. *Pesquisas em Geociências*, 19(1), 1-26.

TRENBERTH, K., CARON, J., STEPANIAK, D. & WORLEY, S. 2002. Evolution of El Nino-Southern Oscillation and global atmospheric surface temperatures. *Journal of Geophysical Research*, 107, 4065, DOI: https://doi.org/10.1029/2000JD000298

TRENBERTH, K., ZHANG, R. & NCAR (National Center for Atmospheric Research Staff) (eds.). 2021. *The Climate Data Guide: Atlantic Multi-decadal Oscillation (AMO)* [online]. Boulder: NCAR. Available at: https://climate-dataguide.ucar.edu/climate-data/atlantic-multi-decadal--oscillation-amo [Accessed: YEAR Mo DAY].

VOUSDOUKAS, M. I., MENTASCHI, L., VOUKOUVALAS, E., BIANCHI, A., DOTTORI, F. & FEYEN, L. 2018. Climatic and socioeconomic controls of future coastal flood risk in Europe. *Nature Climate Change*, 8(9), 776-780, DOI: https://doi.org/10.1038/s41558-018-0260-4

WAN, W., Y., FAN, C., DAI, Y., LI, L., SUN, W. & ZHOU, P. 2018. Assessment of the joint development potential of wave and wind energy in the South China Sea. *Energies*, 11(2), 1-26, DOI: https://doi.org/10.3390/en11020398

WANG, C., LEE, S. K. & ENFIELD, D. B. 2008. Atlantic warm pool acting as a link between Atlantic Multidecadal Oscillation and Atlantic tropical cyclone activity. *Geochemistry, Geophysics, Geosystems*, 9(5), DOI: https://doi.org/10.1029/2007GC001809

WANG, X. L. & SWAIL, V. R. 2000. Changes of extreme wave heights in Northern hemisphere oceans and related atmospheric circulation regimes. *Journal of Climate*, 14(10), 2204-2221.

WANG, X. L., ZWIERS, F. W. & SWAIL, V. R. 2003. North Atlantic Ocean wave climate change scenarios for the twenty-first century. *Journal of Climate*, 17, 2368-2383.

WANG, Y., LI, S. & LUO, D. 2009. Seasonal response of Asian monsoonal climate to the Atlantic Multidecadal Oscillation. *Journal of Geophysical Research*, 114(D2), DOI: https://doi.org/10.1029/2008JD010929

WASEDA, T., WEBB, A., SATO, K., INOUE, J., KOHOUT, A., PENROSE, B. & PENROSE, S. 2018. Correlated increase of high ocean waves and winds in the ice-free waters of the Arctic Ocean. *Scientific Reports*, 8, 4489, DOI: https://doi.org/10.1038/s41598-018-22500-9

YANG, Y. M., AN, S. I., WANG, B. & PARK, J. H. 2020. A global-scale multidecadal variability driven by Atlantic multidecadal oscillation. *National Science Review*, 7(7), 1190-1197, DOI: https://doi.org/10.1093/nsr/nwz216

YOUNG, I. R., ZIEGER, S. & BABANIN, A. V. 2011. Global trends in wind speed and wave height. *Science*, 332(6028), 451-455.

ZHANG, R. & DELWORTH, T. L. 2005. Simulated tropical response to a substantial weakening of the Atlantic thermohaline circulation. *Journal of Climate*, 18(12), 1853-1860, DOI: https://doi.org/10.1175/JCLI3460.1